

GRAVITY: The impact of non-common optical paths within the metrology system

Yitping Kok^{*a}, Stefan Gillessen^a, Sylvestre Lacour^b, Frank Eisenhauer^a, Nicolas Blind^a, Johannes Weber^a, Magdalena Lippa^a, Oliver Pfuhl^a, Leonard Burtscher^a, Ekkehard Wieprecht^a, Thomas Ott^a, Marcus Haug^a, Stefan Kellner^a, Frank Haußmann^a, Eckhard Sturm^a, Annemieke Janssen^a, Reinhard Genzel^a, Guy Perrin^b, Karine Perraut^{c,d}, Christian Straubmeier^e, Wolfgang Brandner^f, Antonio Amorim^g, Oliver Hans^a.

^aMPE, Gießenbachstraße 1, 85748 Garching, Germany;

^bLESIA, Observ. de Paris Meudon, 5, place Jules Janssen, 92195 Meudon Cedex, France;

^cUniv. Grenoble Alpes, IPAG, F-38000, Grenoble, France;

^dCNRS, IPAG, F-38000, Grenoble, France;

^eI. Physikalisches Institut, Universität zu Köln, Zùlpicher Straße 77, 50937 Köln, Germany;

^fMax-Planck-Institut für Astronomie, Königstuhl 17, 69117 Heidelberg, Germany;

^gSIM FCUL, Campo Grande, Edif. C1, P-1749-016 Lisbon, Portugal.

ABSTRACT

The laser metrology system in the GRAVITY instrument plays a crucial role in an attempt at high-precision narrow-angle astrometry. With a design goal of achieving 10 microarcseconds precision in astrometry, the system must measure the optical path difference between two beam combiners within GRAVITY to an accuracy of better than 5nm. However in its current design, some parts of the optical paths of the metrology system are not common to the optical paths of starlight (the science path) which it must measure with high accuracy. This state of the design is true for most but not all the baselines which will be used by the GRAVITY instrument. The additional non-common optical paths could produce inaccurate path length measurements and consequently inaccurate measurements of the differential phase between fringe packets of two nearby celestial objects, which is the main astrometric observable of the instrument. With reference to the stability and the sensitivity of the non-common paths, this paper describes the impact of a biased differential phase measurement on the narrow-angle astrometry and the image reconstruction performance of the GRAVITY instrument. Several alternative designs are also discussed.

Keywords: astrometry, stars: imaging, techniques: interferometric, methods: data analysis

1. INTRODUCTION

The role of a laser metrology system in an optical long baseline interferometer is to measure optical path difference traversed by starlight (or light from celestial targets of interest). In its most basic application, the optical path difference (OPD) of the two arms of the interferometer are measured so that a necessary amount of optical delay can be inserted into either one of the arm to keep the difference close to zero. The amount of optical delay is estimated from the baseline of the interferometer and the position of the source in the sky. However, for astrometric applications, the reverse is done. The optical path difference are measured to estimate the position of the source. For differential astrometry in which only the relative position of two sources is of interest, measurement of the differential optical path difference, dOPD, between two interferometers, each observing one of the two sources, is sufficient. In order to achieve high precision astrometry, the two interferometers are usually designed, but not theoretically necessary, to share the same baseline and most of their optical paths.

The relation between dOPD, and the relative position of two celestial objects, $\Delta\vec{s}$, is,

$$\text{dOPD} = (\hat{s}_1 - \hat{s}_0) \cdot \vec{B} = \Delta\vec{s} \cdot \vec{B}, \quad (1)$$

*E-mail: yitping@mpe.mpg.de

where \hat{s}_1 and \hat{s}_0 are unit vectors pointing to the two objects on sky. The fiducial point where the unit vector points to is straightforward if the target object is an unresolved star. However, if the target object is resolved, the fiducial point which the unit vector points to is the centroid of the intensity distribution projected along the baseline vector. A resolved object is also assumed to be a star or multiple stars hereafter for the sake of keeping the types of object minimal for the discussion in this paper.

The unit vector, \hat{s} , and the baseline vector are usually expressed in the local zenith coordinate frame where the three orthogonal axes x , y and z point to East, North and the zenith respectively. The time-varying unit vector is given as,

$$\hat{s} = \begin{bmatrix} s_x \\ s_y \\ s_z \end{bmatrix} = \begin{bmatrix} -\cos \delta_2 \sin \text{HA} \\ \cos \phi_{\text{LAT}} \sin \delta - \sin \phi_{\text{LAT}} \cos \delta \cos \text{HA} \\ \sin \phi_{\text{LAT}} \sin \delta + \cos \phi_{\text{LAT}} \cos \delta \cos \text{HA} \end{bmatrix}, \quad (2)$$

where $\text{HA} = \text{LST} - \alpha$ is the hour angle of the source while α and δ are the two orthogonal axes in the equatorial coordinate system that describes the position of the source on sky. The acronym LST and ϕ_{LAT} are the local sidereal time and the latitude of the observation site respectively. If a reference star is located at (α, δ) in the equatorial coordinate system and another (target) star is located at $(\alpha + \Delta\alpha, \delta + \Delta\delta)$, then the differential astrometry of the target with respect to the reference is $(\Delta\alpha, \Delta\delta)$. The accuracy of the differential astrometry depends on many factors. Interpreting Eq. (1), they can be generally divided into two categories, i.e. baseline related and optical path length related. Examples of baseline related errors are namely a misalignment of telescope pupils and a drift of telescope pivot point. Examples of optical path length related errors are namely an uncertainty in the metrology light wavelength and a non-negligible difference between the actual and measured path.

GRAVITY is an interferometric instrument under development that will measure the differential astrometry of two celestial objects at ~ 10 microarcseconds (μas) accuracy. It is a two-interferometer instrument that operates in a cohesive and correlated manner through an optical linkage provided by a high precision laser metrology system. The GRAVITY instrument is specified to measure the differential optical path difference between two of its interferometers to an accuracy of 1nm (rms) in 3 minutes.¹ Such a specification would allow it to achieve $\sim 10\mu\text{as}$ astrometric accuracy within that time interval.² Having such an extreme specification, the instrument has numerous design and engineering challenges. Detailed discussion on the many factors limiting the instruments astrometric error budget is given in Ref. 3.

This paper focuses on the accuracy of the differential optical path difference measurement, which is one of the many factors in the astrometric error budget. More specifically, this paper focuses on one of the currently more dominant factors affecting the accuracy of the metrology system, i.e. the non-common path length difference within the GRAVITY instrument. In the instrument's current design, first reported in Ref. 1, there is a non-negligible difference between the actual optical path to be measured (hereafter referred to as the science path) and the optical path that is measured by the instrument's laser metrology system (hereafter referred to as the metrology path). This paper reports on results of laboratory tests on the stability and the sensitivity of the non-common paths between the science and the metrology. This paper also discusses the impact of such biased measurements on the differential astrometry of various types of celestial targets.

2. OPTICAL PATHS

Fig. 1 shows a schematic diagram of the GRAVITY instrument. It has two interferometers that share the same set of telescopes and therefore the same set of (wide-angle) baselines.² They also share most of the optical components until the field splitters, which split light from two stars within the instrument's field of view (FOV) to the two interferometers. The FOV of the instrument is $\sim 2''$ or $\sim 4''$ when it is used with the Unit Telescopes (UTs) or the Auxiliary Telescopes (ATs) of the VLTI. For each interferometer, light is combined with an integrated optics (IO) beam combiner. The beam combiner can combine light from up to 4 telescopes and the optical paths within the integrated optics are shown in Fig. 2(a). The combined light exits the beam combiner via 24 single mode waveguides, i.e. 4 per baseline per fringe.

The waveguides are the location where the metrology laser is injected into an interferometer. The metrology laser is injected into 2 of the 24 waveguides and *from the injection point onwards* it traces the science path in

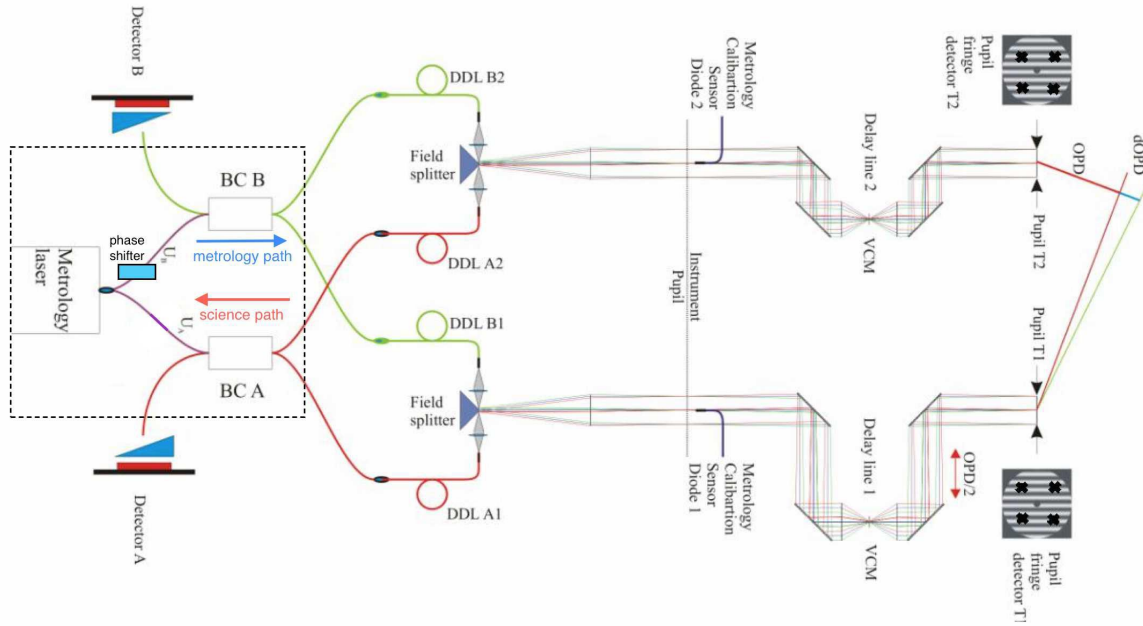


Figure 1: Schematic diagram of the GRAVITY instrument. Starlight enters the instrument through four telescopes (only 2, T1 and T2, are depicted in the diagram) which are shared by two interferometers. The main component of the two interferometers within the instrument is the integrated optics beam combiners (BCA and BCB). Starlight propagates along the science path, which starts at the telescopes (only 2 out of 4, T1 and T2, are depicted) on right side and ends at the detectors on the left side of the diagram. The interferometers share the same set of telescopes and optics until the field splitters. The metrology laser propagates along the metrology path in the opposite direction and forms spatially modulated fringes at the telescope pupils. The fringes encode the differential optical path difference between the two interferometers and phase-shifting interferometry is used to retrieve the path difference. The dashed line box shows the boundary of the Fig. 2(a).

reverse until the pupil plane of the telescopes. The spatially modulated fringes formed across one telescope pupil encode the OPD between two interferometer arms that originate from that particular telescope. The OPD is retrieved using phase-shifting interferometry.⁴ The dOPD between the two interferometers for a given baseline is then the differential phase (in optical path length units) of the fringes across the pupil of two telescopes forming the baseline.

At high accuracy, however, the straightforward relation between the differential phase of the metrology fringes and the dOPD of the two interferometers is valid only for 2 out of the total 6 baselines. This is because there are optical paths, *between the metrology injection point and the metrology laser source*, that are not propagated by the starlight and could affect the differential phase of the fringes at the telescope pupil. Fig. 2 illustrates this. This part of the optical path of the metrology system, labeled as Φ_A and Φ_B in the figure, is commonly referred to as the *non-common optical path (NCP)* because it is not seen by both the starlight and the metrology laser simultaneously. It consists of $\sim 5\text{cm}$ propagation in two single mode optical fibers and $\sim 50\text{cm}$ propagation in vacuum, with the former being the dominant source of optical path difference. The mathematical formalism of the laser metrology system, the NCP length difference and the affected (4 out of 6) baselines are given in Ref. 1. The non-negligible path difference between two metrology injection units is found to be in the order of several nanometers, which is larger than its expected value of $\lesssim 1\text{nm}$.

3. CHARACTERIZATION OF THE NCP LENGTH

The magnitude of the NCP length difference is estimated from laboratory measurements. The laboratory setup consisted of the metrology injection part of only one interferometer. The setup is similar to the one depicted

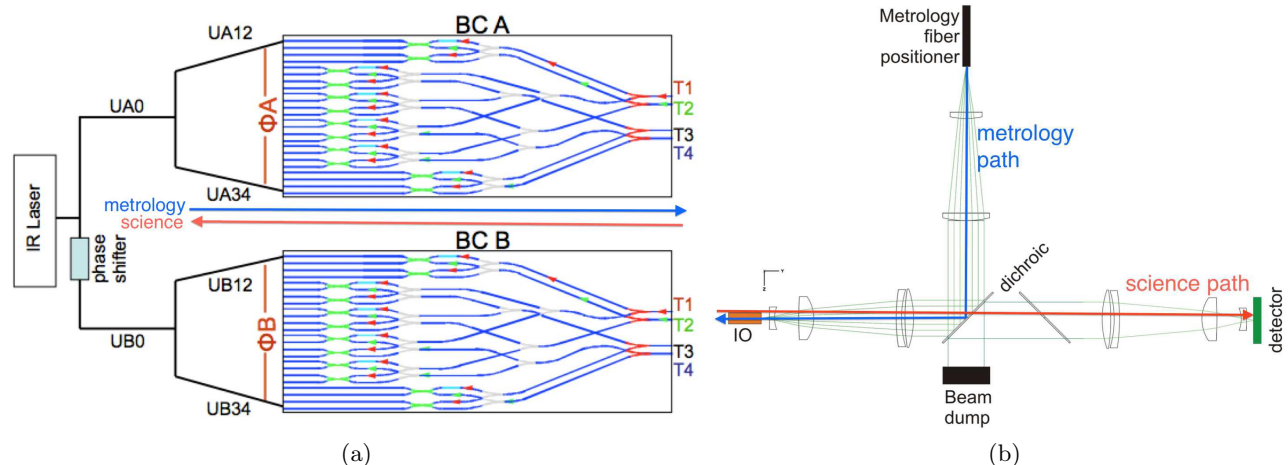


Figure 2: Schematic diagram of (a) the current metrology injection scheme. Each beam combiner has two injection points where the metrology laser is routed to all the 4 telescopes. The optical paths labeled UA12, UA34, UB12 and UB34 are physically similar and the metrology path in (b) shows the optical setup of either one of them. They are also known as the non-common paths in the metrology system because they do not trace the science path which ends after the exiting the beam combiners. Each path consists of a single mode fiber, collimating and focusing lenses. All the components in the diagrams are housed inside an evacuated cryostat. The non-negligible difference between non-common path length of both beam combiners gives rise to a systematic bias in the metrology measurement and consequently the astrometry of the GRAVITY instrument.

in Fig. 2(b) minus the science detector on the right hand side of the diagram. The metrology laser exiting the science entrances of a prototype IO beam combiner are analyzed in the pupil plane with an infra-red camera. One of the four science entrances (or metrology output) is blocked with a metal masked, as shown in Fig. 3(a), so that spatial fringes are formed with 3 apertures. The figure also highlights two paths taken by the metrology laser, injected into two different science exits, within the IO beam combiner. An example interferogram recorded with the infra-red camera is shown in Fig. 3(b). Fringes of 3 redundant baselines as a result of the spacing of the apertures are clearly seen. This Fizeau-interferometer-like setup is described in further details in Ref. 5.

Although the setup represents only half of the NCP it is sufficient because the optical paths are the same (but not strictly identical) in both interferometers. The measured OPD from the metrology fringes represents either Φ_A or Φ_B in Fig. 2(a). The value of the NCP length difference, which is of a concern to the overall metrology system accuracy, is estimated from the OPD measurements in 2 ways. First, the stability of the NCP length difference over a period of time is conservatively estimated as $\sqrt{2}$ times the measured OPD stability because both metrology injection units may experience an uncorrelated thermal drift within the cryostat. Second, the sensitivity of the NCP length difference towards a variation in laser power is estimated to be similar to the measured OPD sensitivity because the induced OPD fluctuation originates from the same source, i.e. the metrology laser.

Two OPD measurements are obtained from each interferogram recorded during a run. One is obtained from the fringes of baseline formed by aperture 1-0 while another from the fringes of baseline formed by aperture 2-0. The fringes of baseline formed by aperture 2-1 originate from the same optical fiber and therefore do not probe the OPD of the two fibers. Despite that, they are used in the data analysis to correct for camera motion. Fig. 4 shows the stability of the OPD over a timescale of several hours while Fig. 5 shows the sensitivity of the OPD towards laser power fluctuation. The absolute value of the OPDs in the plot is ambiguous by an integer number of laser wavelength (1908nm) and therefore is not important. The relative value of the OPDs is the main result. The OPD of one metrology injection unit drifts by $\sim 5\text{nm}$ in 1 hour and varies by $\sim 1.6\text{nm}$ per mW of laser power. Assuming that the NCP length difference cannot be recovered from the metrology data (see Sec. 4), the first number implies that, with the current metrology injection scheme, the fiducial zero of the metrology system

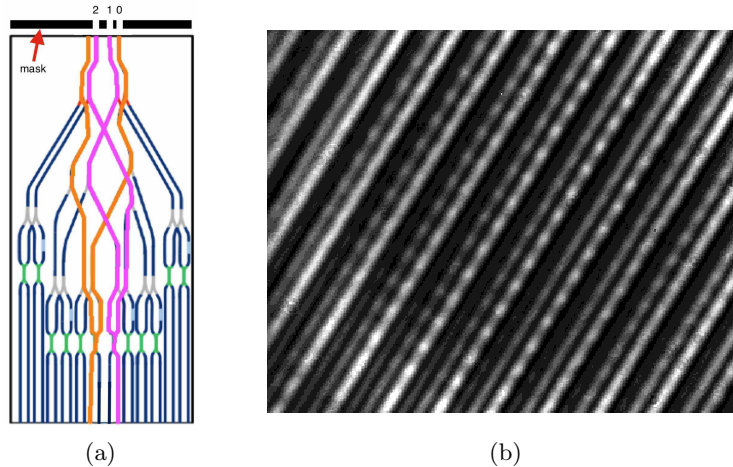


Figure 3: Schematic diagram of (a) the prototype IO beam combiner used for the Fizeau-interferometer-like laboratory setup and (b) the spatially modulated fringes produced. The paths of the metrology laser within the beam combiner, injected at two separate location, are highlighted. A mask selects 3 out of 4 apertures to be used. Laser light exiting aperture 0 originates from one single mode fiber while light exiting aperture 1 and 2 originates from the other fiber of metrology injection unit.

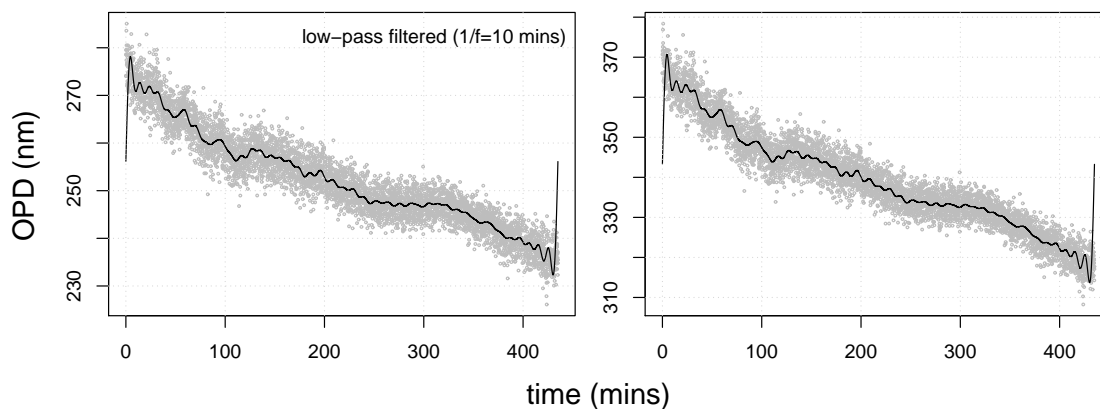


Figure 4: Stability of the OPD (~ 5 nm per hour) of a metrology injection unit. The Fizeau-interferometer-like setup produces 2 sets of OPD measurement (from fringes of baselines 2-0 and 1-0, see Fig. 3) for each interferogram. The temperature difference of the mountings of the two single mode fibers inside the injection unit was controlled to a stability of 3mK while the temperature of the mounting of the IO beam combiner was controlled to a stability of 2mK. The solid line is a low-pass Fourier transform filtered version of the OPD measurements in gray. The cut-off frequency of the filter is $(10 \text{ mins})^{-1}$.

must be reset every ~ 10 minutes or less in order to keep the overall dOPD error within 1nm. The second number implies that the NCP length difference may fluctuate as much as 8nm due to power fluctuation of the metrology laser. The metrology laser is specified to have a power stability of 0.5% (rms) and its nominal operating power is ~ 1 W. The results from the laboratory measurements indicate that the NCP length difference exceeds the expected value of 1nm and may consequently lower the astrometric accuracy of the GRAVITY instrument.

4. IMPACT OF BIASED DIFFERENTIAL OPD MEASUREMENTS

A series of computer simulations were carried out in order to evaluate the impact of biased dOPD measurements on the astrometry of different types of target objects. In order to keep the simulations simple, the bias in the measurement is assumed to arise only from the NCP length difference, which is represented by the symbol Φ_{NCP}

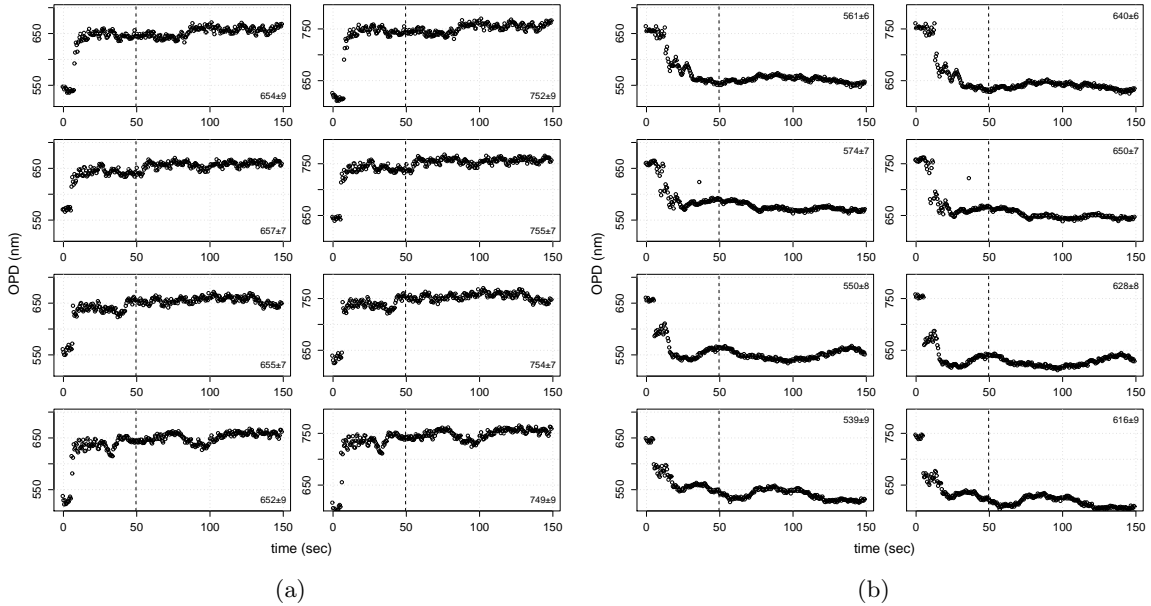


Figure 5: Step responses of the OPD of a metrology injection unit towards a (a) positive and (b) negative change in the laser power. A step of 150mW unpolarized laser power was given at the beginning of the plot and the mean OPD is estimated 50 secs after the step (indicated by the vertical dashed lines). Each row of plots represents a power stepping iteration while each column represents an OPD measurement (2 per iteration) of the injection unit. Sensitivity of the OPD is $\sim 1.6\text{nm}$ per 1 mW laser power (scaled by 2 from the changes see from the plots for polarized laser power).

($= \Phi_A - \Phi_B$) in mathematical expressions that follow hereafter. Baseline related errors² are also assumed to be zero in the simulations and therefore do not affect the astrometry. The nominal reference star for the Galactic Center observations, IRS 16C, was assigned to be the reference star and assumed to be an unresolved single star in all the simulations discussed in the following subsections.

4.1 On unresolved single stars

The most simple target is a single and unresolved star. For such a target, the closure phase of the fringes is zero. That means the fiducial point (or photo-center) where the unit vector points to is the same for all baselines. In this case, the differential astrometry of the target star with respect to the reference star is not affected by the non-common path problem. This is because the differential astrometry is the solution of a mathematical problem of 2 unknowns and the GRAVITY instrument has 6 simultaneously measurements, 2 of which are obtained from baselines that are free from the non-common path problem.

The definition of the 2-unknown problem is as follows. Suppose f represents the quantity $\hat{s} \cdot \vec{B}$ and therefore a function of \vec{B} , α and δ . Then, the differential optical path difference in Eq. (1), can be rewritten as,

$$\begin{aligned} d\text{OPD} = f_\alpha \Delta\alpha + f_\delta \Delta\delta + \\ \frac{1}{2} (f_{\alpha\alpha} \Delta\alpha^2 + f_{\delta\delta} \Delta\delta^2 + 2f_{\alpha\delta} \Delta\alpha\Delta\delta) + \dots, \end{aligned} \quad (3)$$

where f_α and f_δ denote the first order while $f_{\alpha\alpha}$, $f_{\delta\delta}$, and $f_{\alpha\delta}$ denote the second order partial differentiation of $f(\vec{B}, \alpha, \delta)$ with respect to α and δ . If the second and higher order terms are ignored for first order approximation, $\Delta\alpha$ and $\Delta\delta$ can be determined by solving the following linear algebra,

$$\mathbf{d} = \mathbf{B} \mathbf{M} \begin{bmatrix} \Delta\alpha \\ \Delta\delta \end{bmatrix} + \mathbf{c} \Phi_{\text{NCP}}, \quad (4)$$

where $\mathbf{d} = [\widetilde{\text{dOPD}}_1 \ \widetilde{\text{dOPD}}_2 \ \cdots \ \widetilde{\text{dOPD}}_6]^T$ is a column vector of estimated dOPDs and \mathbf{B} is a matrix of baselines on which the dOPDs are measured,

$$\mathbf{B} = \begin{bmatrix} B_{1,x} & B_{1,y} & B_{1,z} \\ B_{2,x} & B_{2,y} & B_{2,z} \\ \vdots & \vdots & \vdots \\ B_{6,x} & B_{6,y} & B_{6,z} \end{bmatrix}. \quad (5)$$

The term $\mathbf{M} \begin{bmatrix} \Delta\alpha \\ \Delta\delta \end{bmatrix}$ is the linearized model of $\hat{s}_1 - \hat{s}_0$ of Eq. (1), where,

$$\mathbf{M} = \begin{bmatrix} \cos \delta \cos \text{HA} & \sin \delta \sin \text{HA} \\ -\sin \phi_{\text{LAT}} \cos \delta \sin \text{HA} & \sin \phi_{\text{LAT}} \sin \delta \cos \text{HA} + \cos \phi_{\text{LAT}} \cos \delta \\ \cos \phi_{\text{LAT}} \cos \delta \sin \text{HA} & -\cos \phi_{\text{LAT}} \sin \delta \cos \text{HA} + \sin \phi_{\text{LAT}} \cos \delta \end{bmatrix}. \quad (6)$$

The HA and declination, δ , in the equation refer to the position of the reference star on sky. The second term in Eq. (4) defines which baselines are affected and unaffected by the non-common path problem. If $\mathbf{c} = [0 \ 1 \ 1 \ 1 \ 1 \ 0]^T$, then the 1st and the 6th baselines are unaffected while the rest are affected. The scalar Φ_{NCP} denotes the length difference between the non-common optical paths. Eq. (4) assumes that the estimated dOPDs have been corrected for constant offsets arising from the metrology measurements.

If \mathbf{K} represents the kernel matrix of \mathbf{c} such that $\mathbf{K}\mathbf{c} = \mathbf{0}$ and \mathbf{W} is the covariance matrix of the estimated dOPDs, then,

$$\begin{bmatrix} \Delta\alpha \\ \Delta\delta \end{bmatrix} = (\mathbf{M}^T \mathbf{B}^T \mathbf{K}^T \mathbf{W}^{-1} \mathbf{K} \mathbf{B} \mathbf{M})^{-1} \mathbf{M}^T \mathbf{B}^T \mathbf{K}^T \mathbf{W}^{-1} \mathbf{K} \mathbf{d} \quad (7)$$

The above formalism represents the linear regression approach of solving for the differential astrometry. Since the second and higher order terms are ignored in such an approach, the accuracy of the solution is limited by the magnitude of those terms.

The approximation error of the solution of $\begin{bmatrix} \Delta\alpha \\ \Delta\delta \end{bmatrix}$ due to higher order terms can be estimated from the second order partial differentiation terms of $f(\vec{B}, \alpha, \delta)$. It can be shown that,

$$\begin{aligned} & \frac{1}{2} (f_{\alpha\alpha} \Delta\alpha^2 + f_{\delta\delta} \Delta\delta^2 + 2f_{\alpha\delta} \Delta\alpha\Delta\delta) \\ &= \frac{1}{2} \begin{bmatrix} B_x \\ B_y \\ B_z \end{bmatrix}^T \begin{bmatrix} -s_x & -s_x & -\sin \delta \cos \text{HA} \\ -s_y + \cos \phi_{\text{LAT}} \sin \delta & -s_y & \sin \phi_{\text{LAT}} \sin \delta \sin \text{HA} \\ -s_z + \sin \phi_{\text{LAT}} \sin \delta & -s_z & -\cos \phi_{\text{LAT}} \sin \delta \sin \text{HA} \end{bmatrix} \begin{bmatrix} \Delta\alpha^2 \\ \Delta\delta^2 \\ \Delta\alpha\Delta\delta \end{bmatrix}, \end{aligned} \quad (8)$$

where the row vector $[B_x \ B_y \ B_z]$ represent one of the 6 baselines in Eq. (5). The coordinates, HA and δ , and the vector components, s_x , s_y , and s_z , in the equation are associated with the position of the reference star on sky. For the case of the VLTI, the approximation error is in the order of several nanometers and several tens of nanometers for on-sky separations of $<2''$ and $<4''$ respectively. These numbers are estimated for a baseline of $\sim 100\text{m}$. The example in Fig. 6 shows the magnitude of the unaccounted optical path differences when a linear dOPD model is used to solve for the differential astrometry of several stars near the Galactic Center. The example shows that a linear model is not suitable for high-precision differential astrometry for widely ($\gtrsim 2''$) separated pair of stars.

In order to avoid an increased in astrometric error, especially for target stars separated by $\gtrsim 2''$ away from a reference star, linear approximation to the differential astrometry model should be avoided. Instead, the actual dOPD model in Eq. (1) should be used. With reference to Eq. (1), the nonlinear regression model for solving the differential astrometry is,

$$\mathbf{d} = f(\mathbf{B}, \alpha + \Delta\alpha, \delta + \Delta\delta) - f(\mathbf{B}, \alpha, \delta) + \mathbf{c} \Phi_{\text{NCP}}. \quad (9)$$

The parameters to solve for are $\Delta\alpha$, $\Delta\delta$ and Φ_{NCP} . The latter can be ignored if it is $\lesssim 5\text{nm}$. Fig. 7(a) shows the astrometric error at various magnitude of Φ_{NCP} if it is ignored and included in the nonlinear regression model.

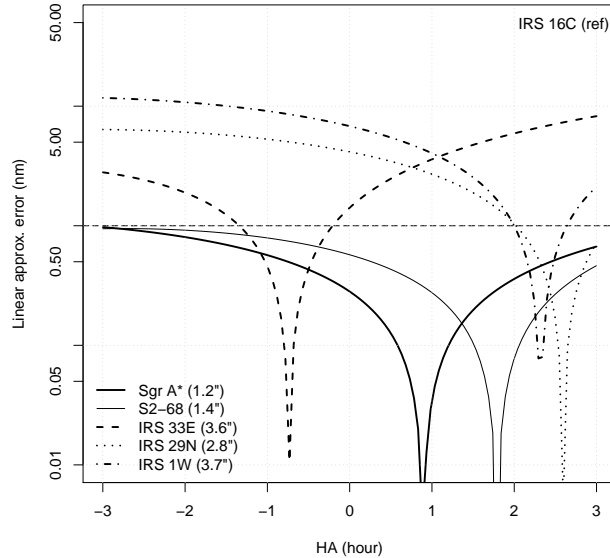


Figure 6: The approximation error of a linear model (estimated with Eq. (8)) at various hour angles of several example stars near the Galactic Center. The differential astrometry, $\Delta\alpha$ and $\Delta\delta$, of each star with reference to a nearby GRAVITY fringe tracking star, IRS 16C, are used to compute the error. The estimated angular separation of the stars from the reference are given in parentheses in the figure. The solid lines indicate stars which are within $2''$ from the reference star, hence observable with the UTs at the VLTI, while the dashed and dotted lines indicate stars which are further away but still within $4''$ from the reference star, and therefore only observable with the ATs. A UT1-UT3 baseline ($\sim 100\text{m}$) is used for this example and the horizontal dashed line indicate the 1nm (or $\sim 2\mu\text{as}$) error threshold.

The errors are obtained from computer simulations of measurements of dOPD when Sgr A* is observed with the UTs at the VLTI. The uncertainty (standard deviation) of the measurements was set to be 1nm , which is the design target of the GRAVITY instrument over a time interval of 3 minutes. The uncertainty of each point in the plot shows the dispersion of the extracted parameters within 1000 iterations. Fig. 7(a) also shows that the astrometric errors are systematically lower for one of the two different arrangements of telescopes. This is because arrangement with the lower astrometric errors, UT1-UT3-UT2-UT4, which forms baseline #1 with UT1 and UT3, baseline #2 with UT1 and UT2, and so on, has the 2 baselines that are unaffected by the non-common path problem relatively longer than the others. The projected baseline vectors on the uv -plane of the two arrangements are shown in Fig. 7(b). The unaffected baseline vectors are represented by the solid lines in the figure.

Although the presence of non-common paths introduced biases in the dOPD measurements, the differential astrometry of a single star is unaffected by it due to the redundancy of baselines in the GRAVITY instrument.

4.2 On unresolved binary stars

If the target is a binary star then the non-common path term cannot be simultaneously recovered with the differential astrometric parameters from the data because the closure phase of such a target is no longer always zero. The photo-center of the target varies with the orientation of the baseline used to observe the fringes. The phase shifts introduced by the additional component star of the binary to the fringes of the primary and the biased differential phase measurements due to the NCP length difference are degenerate. Therefore the NCP length difference may falsely appear as a shift in the fringe phase and vice versa. Fig. 8 shows the theoretical amount of phase shifts in optical path length units (in nm) as a function of the separation of the two component

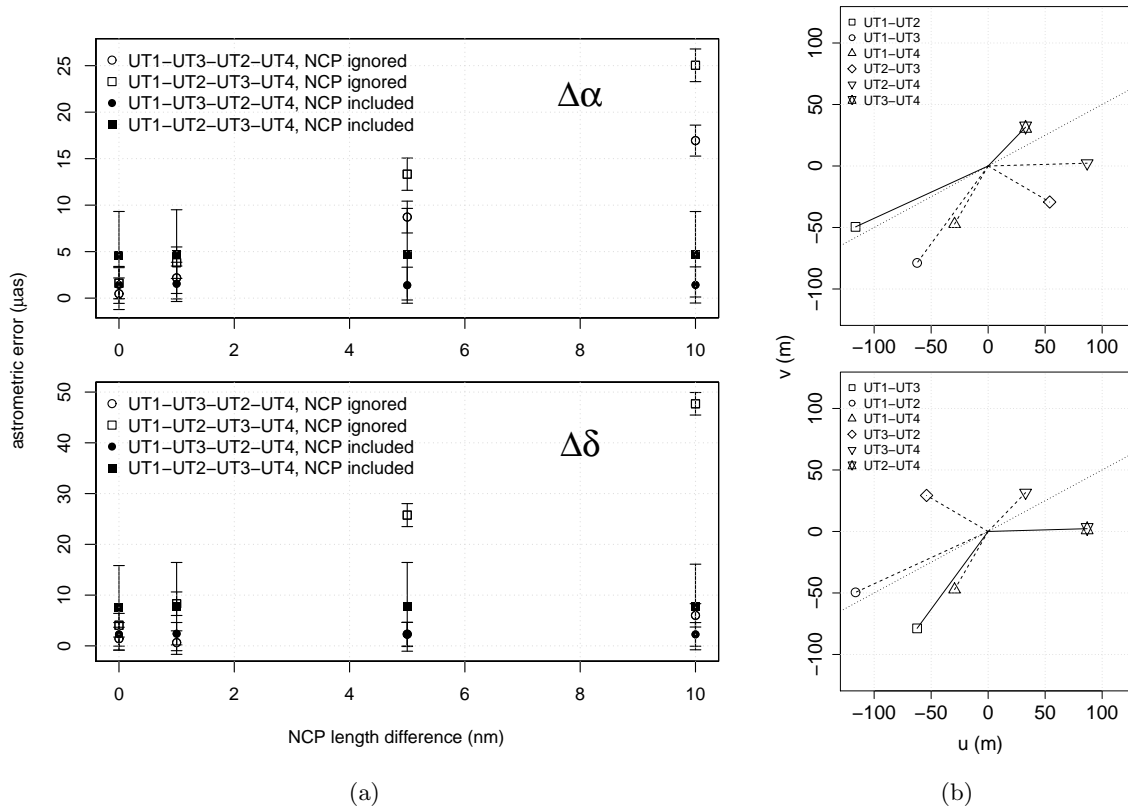


Figure 7: Astrometric errors due to various NCP length difference. The errors in (a) are obtained from computer simulations by computing the difference between the extracted and the expected (input) differential astrometry of Sgr A* with reference to IRS 16C (at HA=1h). The dOPD measurement uncertainty of 1nm is used in the simulation. Larger uncertainties would only scale the error bars of each point by a factor proportional to the baselines of the interferometer. The parameter extraction used a nonlinear regression model given in Eq. (9). The non-common path term, Φ_{NCP} , is non-negligible beyond $\sim 5\text{nm}$ and should be included into the model as one of the parameters to be solved for. The effect of different telescope arrangement towards the astrometric error is also shown. The resulting baseline vectors in the uv -plane are shown in (b). Baseline vectors unaffected by the non-common-path problem are plotted with solid lines while the others are plotted with dashed lines. The dotted lines indicate the position angle of the target with respect to the reference star.

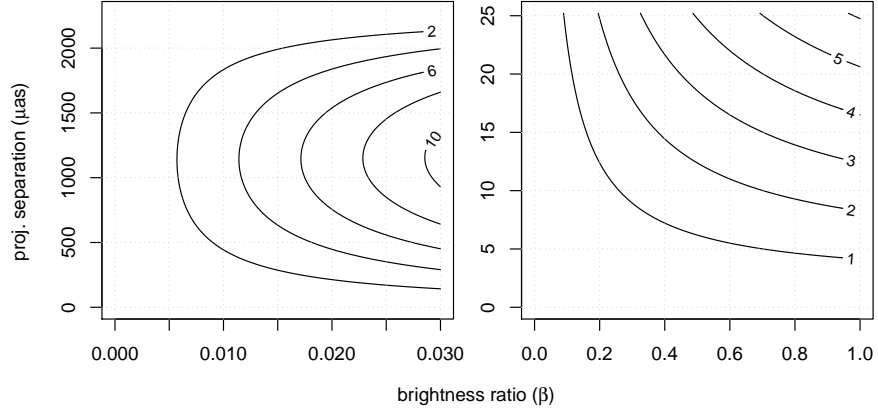


Figure 8: Theoretical amount of phase shift introduced by a secondary component star in a binary to the fringes of the primary. The phase shift, represented by the contour lines and quoted in nm, depends on the projected separation and the brightness ratio, β , of the binary. The phase shift is computed for a wavelength of $2.2\mu\text{m}$ (K -band). The range of the y -axis of the left plot is equivalent to the half a fringe over a 100m baseline. The amount of phase shift is periodic over this range projected separation.

stars projected onto the baseline used for the interferometry and the brightness ratio of the components. The brightness ratio, usually denoted by the symbol β , has values between zero and unity ($0 \leq \beta \leq 1$).

With a targeted dOPD measurement uncertainty of $\sim 1\text{nm}$, a binary star that has a brightness ratio of $\lesssim 0.005$ will still appear as a single star to the GRAVITY instrument and the linear or nonlinear model in the previous section can still be used to extract the differential astrometry of the target object. However, a different nonlinear model must be used for binary stars with larger brightness ratio.

In the case of a binary with a larger brightness ratio and unresolved component stars, the most basic nonlinear model that describes the complex fringe visibility of a binary star target can be shown to be,

$$\mathcal{V} = \exp\left(-i2\pi\sigma \Delta\vec{s} \cdot \vec{B}\right) \left[1 + \beta \exp\left(-i2\pi\sigma \Delta\vec{s}_{1,2} \cdot \vec{B}\right)\right] \quad (10)$$

where $\Delta\vec{s}_{1,2} = \hat{s}_2 - \hat{s}_1$, similar to the definition in Eq. (1), is the relative position of the secondary component with respect to the primary component of the binary. The wavelength of light in which the measurements are carried out are represented by its reciprocal, σ , the mean wavenumber of light. The complex fringe visibility for this particular model is a function of 5 parameters, namely $\Delta\alpha$, $\Delta\delta$, $\Delta\alpha_{1,2}$, $\Delta\delta_{1,2}$ and β . The simplicity of this model is exploited to explore the impact of the non-common path induced dOPD error. A set of simulated noisy complex visibilities of a fictitious binary star ($\Delta\alpha_{1,2} = 13\text{mas}$, $\Delta\delta_{1,2} = -8\text{mas}$) at the position of Sgr A* on sky are generated for a given range of NCP length difference and measurement uncertainties. The mean value of each parameter is extracted from 1000 regression iterations. In each iteration, a different set of complex visibilities are generated. The differences between the extracted and expected position of the primary star with respect to the reference star, IRS 16C, are shown in Fig. 9.

The figure shows a comparison of errors from two slightly different model. Those plotted on the upper row had the parameters extracted without taking into account of the NCP length difference while those plotted on the lower row had the parameters extracted simultaneously with the NCP length difference. The accuracy of the astrometry from the latter regression is much worse than from the former due to the degeneracy mentioned above. It also shows that the NCP length difference must be kept small ($< 5\text{nm}$) if the astrometric error is to be kept $\lesssim 10\mu\text{as}$.

4.3 On extended objects

If the target is resolved, the differential astrometry between its photo-center and the reference star is limited by the magnitude of the NCP length difference. Such an impact is similar to the case of a binary star in the

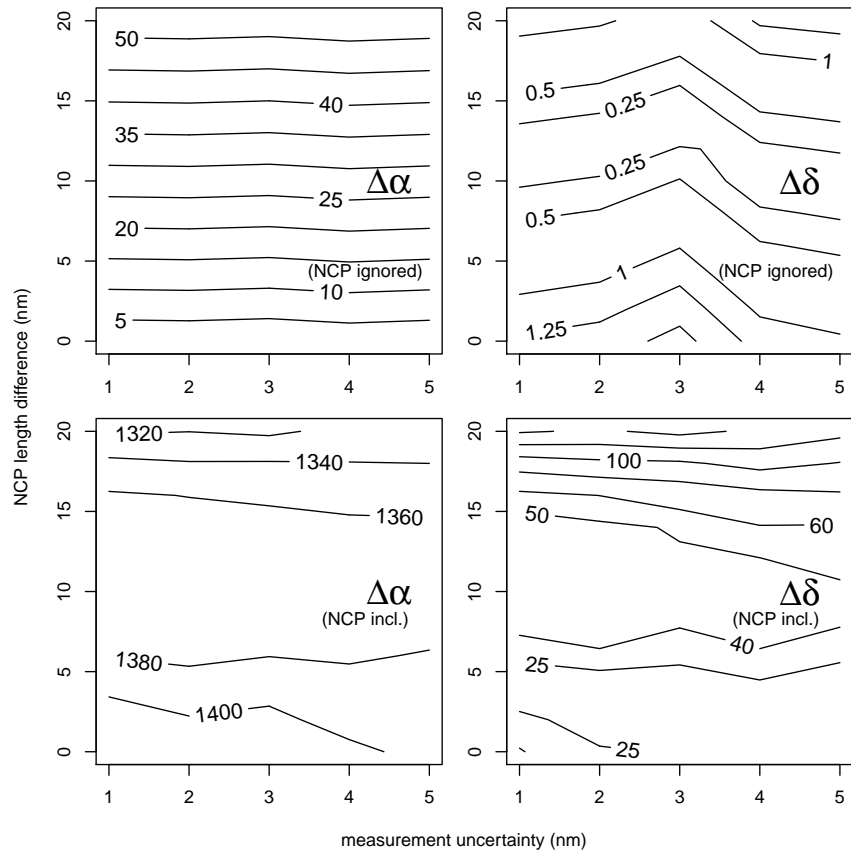


Figure 9: Astrometric error of the primary component of a fictitious binary when observed with UT1, UT3, UT2 and UT4 under various simulated NCP length difference and measurement uncertainties. The uncertainty of squared visibility measurements is 0.01. The contour lines are labeled in units of μas and they represent the mean astrometric error from a sample of 1000 datasets. The astrometry of the component was extracted with (lower row) and without (upper row) taking the NCP length difference into the model fitting process. Doing the former does not necessarily produce smaller error because the additional phase shifts introduced by the secondary component star and the NCP length difference are degenerate. The binary was set to reside at Sgr A* position on sky and had a separation of ($\Delta\alpha_{1,2} = 13\text{mas}$, $\Delta\delta_{1,2} = -8\text{mas}$) in the simulation.

Table 1: Astrometric error (in μas) of different types of targets at various level of Φ_{NCP}

Target type\ Φ_{NCP}	<2nm	<5nm	$\geq 10\text{nm}$
Unresolved single star	<5	<10	<10
Unresolved binary star	$\lesssim 5$	<10	>20
Extended objects	<5	<20	>40

previous subsection. However, if the target has extended and non-point-symmetrical features, then the impact of the NCP length difference on the astrometry cannot be easily investigated with closed form models. Instead an image reconstruction approach is used. A similar investigation has been carried out in Ref. 6 to find out the astrometric accuracy of the imaging-mode of the GRAVITY instrument but only random errors were considered.

An interferometer produces a high-resolution image of the target by means of the aperture-synthesis technique. According to the Van Cittert-Zernike theorem, the Fourier transform of the intensity distribution of a source is equal to the complex visibility of the fringes formed by a given baseline. The image of the target can be reconstructed by taking the inverse Fourier transform of the measured complex visibilities (although a more complicated data analysis is required in practice). The accuracy of the relative position of the features in the reconstructed image depends on the accuracy of the phase component of the complex visibility. In order to gauge the impact on the relative position of astrophysical features in a reconstructed image due to the NCP length difference, an image of a fictitious triplet star at the location of Sgr A* on sky is used as the target for an image reconstruction exercise using biased dOPD measurements. The image of the triplet star is shown in Fig. 10(A).

First, the image is used to generate noisy complex visibility measurements with different VLTI baselines and NCP length differences. A total of 1000 sets of simulated observations are generated for each scenario. Then, the measurements are used to reconstruct the image of the triplet using the MiRA image reconstruction software.⁷ Finally, the centroid position of the reconstructed image of each component star is determined and relative positions of two other component stars with respect to the primary star are computed. The range of NCP length difference inserted into the simulation is between 1nm and 200nm. The dOPD and fringe visibility measurements are generated for observations from hour angle of -2 to 2 and the uncertainties are set to 10nm and 0.01 respectively. Images are reconstructed with the modulus and the argument of the complex visibilities, not with closure phases, because the GRAVITY instrument has two interferometers and is able to measure the complex fringe visibility of a target by means of on- or off-axis phase-referencing. Nonetheless, as an experimental control, several sets of images are also reconstructed with closure phases. The image reconstruction routine is iterated over every set of observations and the mean and standard deviation of the positions are recorded for analyses.

Fig. 11 shows the differences between the relative position of the two other component stars with respect to the primary measured from the reconstructed and the original image. The absolute differences are less important because they are effects of other factors, e.g. the image reconstruction algorithm used, the baselines of the interferometer, phase constants introduced by pixelation of the original image, etc. The relative position of the points on the plots in the figure, showing a linear trend (indicated by the solid and dashed lines), is more important as it reveals the effect of the NCP length difference. In general, the stability of a feature in a reconstructed image, indicated by the trend lines depending on the arrangement of telescopes and the baselines of the interferometer. From the limited number of cases simulated, the stability along a given axis, is $<4\mu\text{as}$ per 1nm of NCP length difference. This number can only serve as an estimation as the simulation carried out has not been sufficiently exhaustive as far as different baselines and the position angles of the component stars are concerned.

5. DISCUSSIONS

Table 1 summarizes the impact of the non-common paths in GRAVITY on the astrometric accuracy of the instrument. However, the astrometric error listed in the table by no means indicates the overall accuracy because other factors were not taken into account. Furthermore, the NCP length difference is assumed to be non-recoverable for targets other than unresolved single stars from the data reduction. This might not be the case.

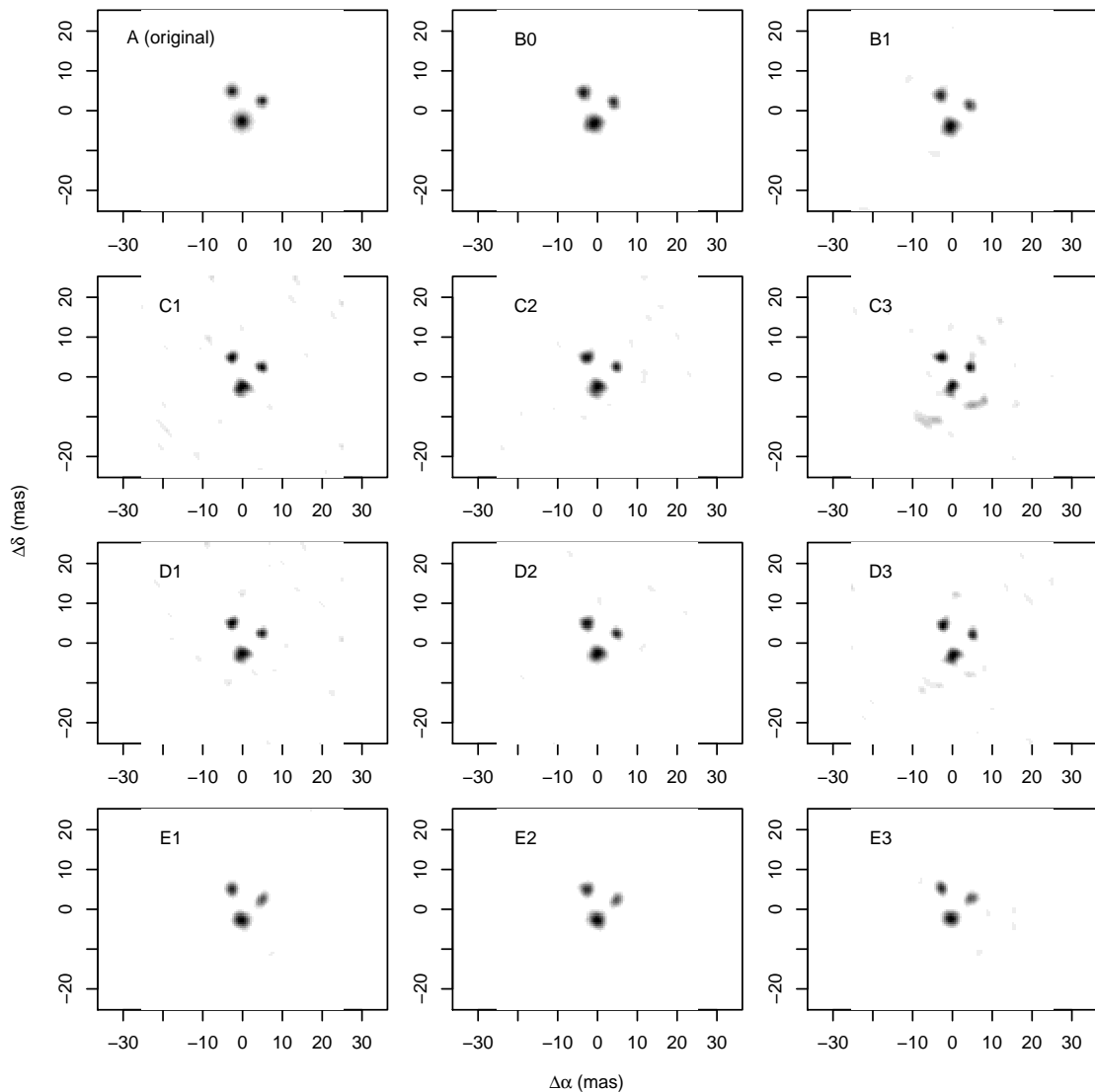


Figure 10: Reconstructed images of a fictitious triplet star at Sgr A* location on sky using the aperture-synthesis technique and the MiRA software.⁷ Images labeled C, D and E are reconstructed with complex visibilities while images labeled B are reconstructed with closure phases. The closure phase uncertainties used in B0 and B1 are 1° and 2° respectively. The phase uncertainties of the complex visibilities (in optical path length units) used C0–C2, D0–D2 and E0–E2 are 1nm, 10nm and 100nm respectively. The uncertainty of the squared visibilities is 0.01. Complex visibility data for C0–C2 and D0–D2 are generated with the UTs while data for E0–E2 are generated with the ATs (all other conditions remained the same). The uv tracks of the baselines from which the complex visibilities are derived are plotted in Fig. 11(d)–(e) respectively.

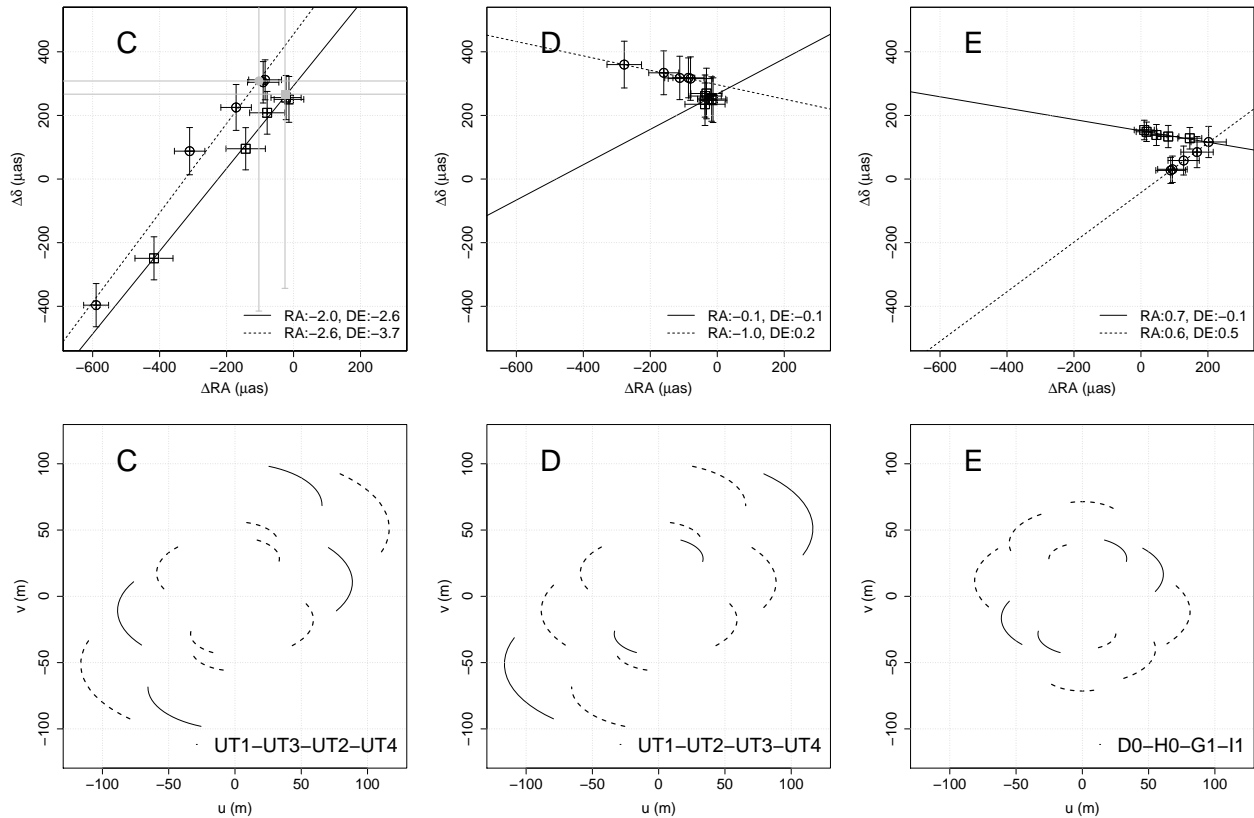


Figure 11: The differences between relative positions of component stars in the reconstructed (C,D,E) and the original images (A) in Fig. 10. Their linear dependence on the NCP length difference are indicated by the numbers at the bottom right corners of the upper row plots. The numbers, given in units of μas per nm, are the slope of the linear trend lines in the plots over a range of 1–200nm of NCP length difference. The uv tracks of the baselines from which the complex visibility data are generated are plotted in the lower rows. The gray points in the plot labeled C are the position differences obtained from images reconstructed with closure phases. The larger error bars are probably due to the $2\times$ lesser number of closure phases versus complex visibility phases.

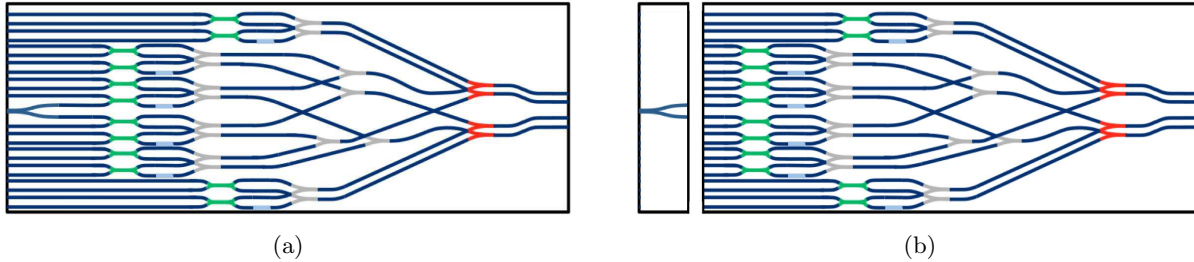


Figure 12: Schematic diagram of (a) an alternative IO beam combiner design which has a Y-junction as one of its light exits and (b) a separated Y-junction with the existing IO beam combiner. Such a design reduces the NCP length difference because the splitting of laser light occurred on an integrated optics chip where the temperature difference between the 2 branches after the splitting can be better controlled.

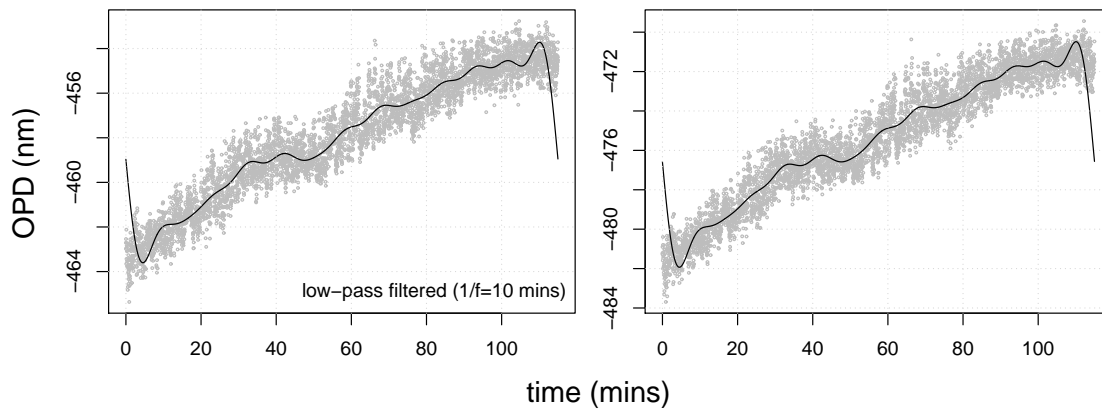


Figure 13: Similar to Fig. 4 except that a modified (with a Y-junction IO beam combiner) metrology injection unit was used for the OPD measurement. Temperature stability of the mountings of the single mode fiber (only one is needed) and the IO beam combiner were controlled to a level of 2mK.

In any case, the numbers in the table suggest that the accuracy of the instrument, for the targets other than unresolved single stars, is likely to exceed the design goal of $10\mu\text{as}$ with the current metrology injection scheme. In view of this impact, there are currently 4 proposed solutions to reduce or preferably eliminate the non-common paths from the instrument altogether.

Firstly, the metrology laser power can be actively controlled so that the fluctuation is reduced from its current specified level. In order to implement this fix, the metrology laser would need to be upgraded to support external control signals and installation of two new power meters or sensors are needed at the metrology injection units. This fix requires the least hardware modification among the available proposals in the time of writing but the metrology laser upgrade is costly. Furthermore, the performance of an external controller has to be investigated.

Secondly, the splitting of the metrology laser in the injection unit can be moved from its current position, at an external IO beam splitter, to the IO beam combiner, thereby eliminating the usage of two single-mode fibers and the dominant source of the NCP length difference. A new IO beam combiner that incorporates a Y-junction as one of its light exits is currently being investigated and Fig. 12(a) shows this new design. The exit of the Y-junction is the new injection point of the metrology laser. Having the light splitting to the telescopes as close as possible and on the integrated optics allows the optical path between the branches to be better controlled. A prototype of this IO beam combiner has been tested with the same laboratory setup and the measurements show promising OPD stability and sensitivity towards laser power. Fig. 13 shows the stability while Fig. 14 shows the step response of the OPD of modified metrology injection scheme towards a laser power change. The sensitivity is $<0.1\text{nm}$ per mW of laser power and the estimated variation in NCP length difference due to a 0.5% (rms) fluctuation in laser power is $<0.5\text{nm}$. Such an amount of variation fits well with the budgeted accuracy

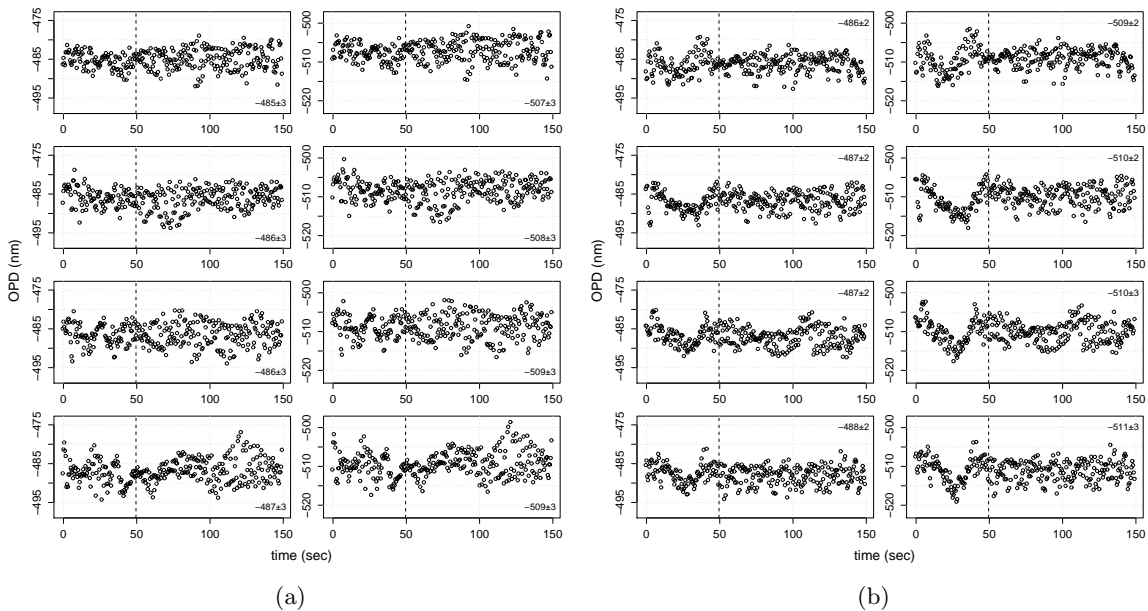


Figure 14: Similar to Fig. 5 except that a modified (with a Y-junction IO beam combiner) metrology injection unit was used for the OPD measurement.

for the metrology system. However, having a Y-junction on the IO beam combiner implies 2 drawbacks. First, the phase error of the science fringes will depend on how well the phase shifts of the remaining 3 exit waveguides are known from offline characterizations. Second, the science flux for the affected baselines will be reduced and may consequently reduce the limiting magnitude of the instrument.

Thirdly, an IO beam splitter custom built to match the dimension of the IO beam combiner can be used in place of the existing one which require the light coupling to the latter to be carried with single mode fibers. This design is a variant of the second proposal above where the Y-junction is cut out from the beam combiner. Fig. 12(b) illustrates this. The performance of the separated Y-junction is expected to be similar to the one attached to the beam combiner but it has yet to be characterized. The drawback of this solution is the limited number of degree of freedom required to align the separated Y-junction and couple the light between it and the IO beam combiner.

Lastly and ideally, the OPD of the non-common path of each injection unit can be directly measured by utilizing the unused laser light that is currently being dumped away. The two fibers in the injection unit produce spatially modulated fringes at the location of the beam dump (see Fig. 2). With the fibers at their nominal positions, which is $\sim 360\mu\text{m}$ apart, there are ~ 17 fringes per 10mm at the beam dump location. Using a linear array of photodiodes, which are usually fabricated in $25\mu\text{m}$ or $50\mu\text{m}$ pixel pitch (active area of one diode) and up to 1024 pixels per array, there would be about 20 or 10 samples per laser fringe and up to ~ 90 fringes per array that can be recorded. Since $\sim 40\%$ of the laser power are not used for the metrology system, a neutral density of the order of at least 6 is needed in order to not saturate the photodiodes. The accuracy of the estimated fringe phase is therefore photon noise and linearity limited. Besides being able to measure the OPD of the two fibers, which is the part that contributes the most to the NCP length difference, this solution retains the metrology injection scheme as it is. There will be no loss of science flux and waveguide which is the case for the Y-junction IO beam combiner solution. The drawback of this solution is extra development time that will incur to install the hardware and build the software to support it.

6. CONCLUSIONS

The non-common path length difference between two metrology injection units is found to be larger than previously estimated. Laboratory measurements estimate the non-common path length difference to be $>1\text{nm}$.

Although 2 out of 6 baselines within the GRAVITY instrument are not affected by the non-common path problem, the effect it has on the astrometry of basic targets (e.g. close binary stars with unresolved components) is apparent through computer simulations. Several modifications to the current metrology injection design have been proposed and are under further investigation so that the astrometric accuracy of the instrument can achieve its design goal of $10\mu\text{as}$ for all types of targets.

REFERENCES

- [1] Gillessen, S., Lippa, M., Eisenhauer, F., Pfuhl, O., Haug, M., Kellner, S., Ott, T., Wieprecht, E., Sturm, E., Haußmann, F., Kister, C. F., Moch, D., and Thiel, M., “GRAVITY: metrology,” in [Proc. SPIE], **8445** (July 2012).
- [2] Lacour, S., Eisenhauer, F., Gillessen, S., Pfuhl, O., Woillez, J., Bonnet, H., Perrin, G., Lazareff, B., Rabien, S., Lapeyrere, V., Clenet, Y., and Kok, Y., “The baseline paradox of optical interferometry. Application to the GRAVITY astrometric error budget,” *ArXiv e-prints* (Apr. 2014).
- [3] Lacour, S., Eisenhauer, F., Gillessen, S., and Perrin, G., “Error budget,” in [Proc. SPIE], **9146** (June 2014).
- [4] Lippa, M., Blind, N., Gillessen, S., Kok, Y., Weber, J., Eisenhauer, F., Pfuhl, O., Janssen, A., Haug, M., Haußmann, F., Kellner, S., Hans, O., Wieprecht, E., Ott, T., Burtscher, L., Genzel, R., Sturm, E., Hofmann, R., Huber, S., Huber, D., Senftleben, S., Pflüger, A., Greßmann, R., Perrin, G., Perraut, K., Brandner, W., Straubmeier, C., Amorim, A., and Schöller, M., “The GRAVITY metrology system: narrow-angle astrometry via phase-shifting interferometry,” in [Proc. SPIE], **9146**, 72 (June 2014).
- [5] Weber, J., Blind, N., and Kok, Y., “Test and optimization of the GRAVITY laser metrology injection,” in [Proc. SPIE], **9146**, 63 (June 2014).
- [6] Vincent, F. H., Paumard, T., Perrin, G., Mugnier, L., Eisenhauer, F., and Gillessen, S., “Performance of astrometric detection of a hotspot orbiting on the innermost stable circular orbit of the Galactic Centre black hole,” *MNRAS* **412**, 2653–2664 (Apr. 2011).
- [7] Thiébaud, E., “MIRA: an effective imaging algorithm for optical interferometry,” in [Proc. SPIE], **7013** (July 2008).